www.rericjournal.ait.ac.th

The Impact of Cooling Channels and Heat Spreaders on the Performance of Proton Exchange Membrane Fuel Cells (PEMFC)

Keoagile Mogorosi*, #, 1, M. Tunde Oladiran*, and Edward Rakgati#

ARTICLE INFO

Article history:
Received 17 February 2022
Received in revised form
30 June 2022
Accepted 01 September 2022

Keywords:
CFD
Cooling
Experiment
Heat spreaders
PEM fuel cell

ABSTRACT

Investigation of the operational behavior of fuel cells is required to assess their overall performance and dynamic stability. This research paper describes the use of Computational Fluid Dynamics (CFD) in investigating the effect of incorporating a separate adjacent cooling channel and heat spreader in a fuel cell. The objective of the study was to find the effect of adding coolant channel and heat spreader to the fuel cell. This model was run using different variables, namely pressure, voltage, and fuel flow rate. The study shows performance of the fuel cell regarding temperature changes, distribution, and water mass fraction changes at a common plane across all the models. The results indicate that the presence of a separate cooling channel and a cooling channel with a heat spreader reduce the local temperatures on the cathode side by about 10°C and 12°C, respectively. The results of the model cells were enhanced by the introduction of cooling channels and heat spreaders.

1. INTRODUCTION

There are global environmental concerns due to harmful gas emissions into the atmosphere from combustion processes. The hydrocarbon fuels are not renewable and are unevenly distributed in various regions of the world. There is an urgent need for inexhaustible fuels to replace the harmful thermal processes. Fuel Cells are attractive alternatives to fossil-based energy resources which have had a head start as compared to most cleaner energy systems and hence are more commercially viable. Fuel cells are electro-chemical devices converting energy into power, heat, and water.

Fuel cell technology is not as competitive commercially as fossil fuel-based systems because of several issues including thermal and water management problems. Thermal issues require introduction of some cooling techniques that would not affect the performance of the fuel cell negatively. Local temperature distributions also present some performance issues. This calls for stringent thermal management measures by redistributing the heat produced by the fuel cell and hence maintain a suitable working temperature. This can be achieved by employing some cooling strategies in heat spreaders and air cooling *etc*. [1]. Mass transport and water management are also critical issues in the positive performance of the fuel cell.

To develop and implement the PEMFC technology efficiently, mathematical modelling of the fuel cell is needed so that both the fuel cell's thermal and water management issues can be investigated and predicted at the design stage. This can be done by means of computer simulations using different load currents, pressure of reactant gases and flow rates of hydrogen gas.

There are several computational fluid dynamics (CFD) models related to this study carried out on PEMFC. For example, Ionescu [2] presented model which investigated the cathode gas flow velocity influence on the performance of the fuel cell. This model also studied the impact of channel height and channel width on the cell current density at a voltage of 0.5V and at varying cathode air flow velocities ranging from 0.04 to 0.42 m/s. In this study water molar and oxygen concentrations at the cathode catalyst layer were also investigated at various gas channel geometries.

Carcadea *et al* [3] presented a CFD model to study the sensitivity of the performance of the fuel cell to the depth and width of the parallel flow channels at the cathode of PEM fuel cell. The models also explored the impacts of operating conditions like pressure, temperature, relative humidity on fuel cell performance.

Wu *et al*. [4] presented the performance of a 3-dimensional model of PEMFC utilizing various numbers of rectangular ribs inserted on the middle in the cathode and anode channels. They determined the resulting cell power. Their results showed that highest net cell power happens for the 5 rectangular ribs which is higher by 6.6 % than the result with no ribs.

Liu *et al*. [5] presented a study to enhance the dimensions of the flow channel of a fuel cell. In their model they investigated the ideal flow channel total width and the wall to rib and rib to the total width ratios,

* Department of Mechanical and Energy and Industrial Engineering, Botswana International University of Science and Technology. Private Bag 16, Palapye, Botswana.

Botswana Institute for Technology Research and Innovation, Private Bag 0082, Gaborone, Botswana.

1 Corresponding author;
E-mail: kemogorosi@gmail.com

for high power densities. They found out that a reduced total width and reduced rib to total width ratio (Lr/Lo) are good for producing high power densities. They observed that a reduction of the ratio Lr to Lo from 1/2 to 1/5 resulted increasing maximum power density by 43 %.

Lee *et al.* [6] studied a 3-dimensional model for a PEM fuel cell that could work with anode and cathode flows simultaneously. They concluded that the oxygen and water concentrations on the center of micro-parallel channel and GDL with varying relative humidities at cathode were considerably affected by the electro-chemical reaction, back diffusion, and electro-osmotic drag.

2. PEMFC TRANSPORT PROCESSES

The domains for transport processes are the anode current collectors (with gas channels), GDL (anode and cathode), catalyst layers (CL)s (anode and cathode), membrane, current collectors (anode and cathode with gas channels), as illustrated in Figure 1.

Hydrogen fuel is transported to the anode of the fuel cell through the channels. Hydrogen is then broken into electrons and protons with the help of a catalyst. The produced protons flow via the proton exchange membrane (PEM) to the cathode. Electrons then travel along an outside load circuit towards the cathode side, hence generating an output current of the cell. On the other side, oxygen (O_2) stream is transported to the cathode. O_2 molecules then react with the incoming protons infusing through the membrane and the electrons coming through the load circuit producing water as shown in Figure 2.

These transport activities across the domains are governed by conservation equations. which are fundamental in the fluid mechanics analysis of the fuel cell and other similar systems. The governing equations also help in modeling fuel cells to predict the performance of the systems.

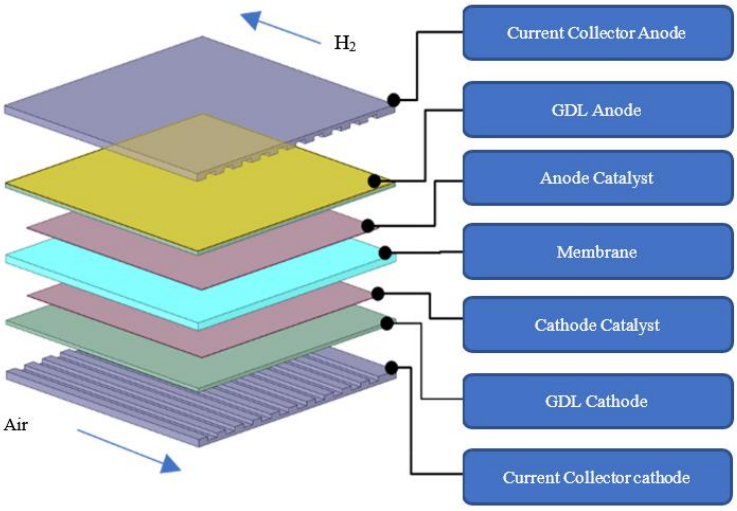

Fig. 1. PEMFC transport domains.

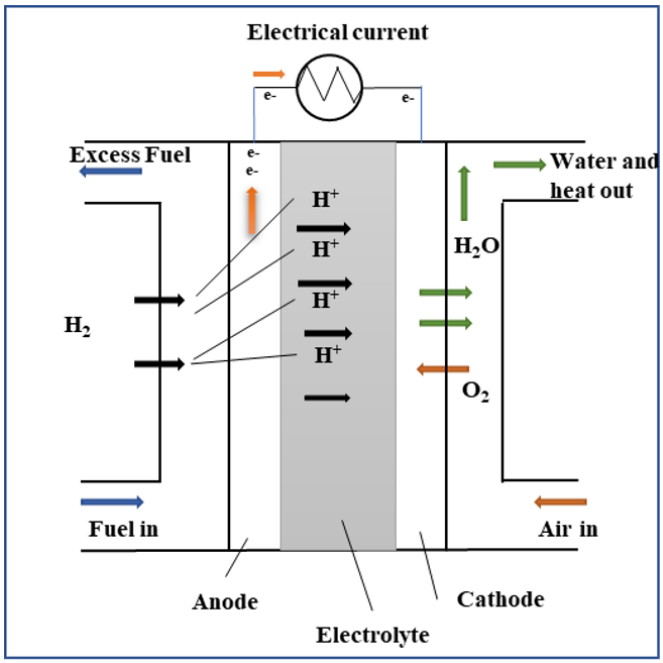

Fig. 2. Transport processes inside a fuel cell.

2.1 Mass Transport Process

The continuity equation for all the species transports therefore accounts for change in density across the fuel cell and is shown by Equation 1[7].

$$\frac{\partial(\rho\varepsilon)}{\partial t} + \Delta(\rho \boldsymbol{v}) = S_m \tag{1}$$

The mass transport source term S_m is taken as zero in the flow-channels since there are no reactions there [5]. So, Equation 1 reduces to:

$$\Delta(\rho v) = 0 \tag{2}$$

The equation is valid for such processes as diffusion, fluid flow, electro-chemical reactions, and phase changes.

2.2 Momentum Transport Process

Momentum transport is normally represented by Navier-Stokes equations describing the flow of incompressible Newtonian fluid applied in the GDLs, catalyst layers and flow field plates [8]. Therefore, fluid velocities in the GDLs, flow channels and also the partial pressures of the species are solved by Equation (3) [9], [10] in which laminar flow is assumed.

$$\frac{\partial(\rho \boldsymbol{v})}{\partial t} + \nabla \cdot (\rho \boldsymbol{v}\boldsymbol{v}) = -\nabla \boldsymbol{p} + \nabla \cdot (\mu^{eff} \nabla \boldsymbol{v}) + S_{mm} \tag{3}$$

The momentum source term S_{mm} allows the equation to be valid for both the porous layers and the flow ducts and is 0 in other regions apart from GDLs and the CLs where it is given by Equation 4 [9],

$$S_{mm} = -\frac{\mu}{K_p}\varepsilon v \tag{4}$$

Regarding water flow in the membrane, an extra source term is the electro-kinetic permeability given by Equation 5 [9].

$$S_m = \frac{\mu}{K_p}\varepsilon_m x_m v + \frac{K_f}{K_p} c_f n_f F \nabla \phi_m \tag{5}$$

2.3 Species Transport Process

The conservation of species (*ie*. hydrogen, water, Nitrogen) is defined by Equation 6.

$$\frac{\partial(\varepsilon \rho y_j)}{\partial t} + \nabla \cdot (\rho \mathbf{v} y_i) = \nabla \cdot \left(\rho D_j \nabla y_i\right) + S_j \tag{6}$$

D_j is calculated by using Equation 7 [9],

$$D_j = \varepsilon_{eff}^{1.5} D_j^o \left(\frac{P_0}{p}\right)^{\gamma_p} \left(\frac{T}{T_o}\right)^{\gamma_t} \tag{7}$$

Where,

$$\varepsilon_{\,eff} = \varepsilon(1 - s) \tag{8}$$

The consumption of reactant species, hydrogen, oxygen and the production of water and heat are defined by Equations 9, 10 and 11 respectively [9],

$$S_{H_2} \frac{M_{w,H_2}}{2F} R_{an} \tag{9}$$

$$S_{O_2} = \frac{M_{w,O_2}}{2F} R_{cat} \tag{10}$$

$$S_{H_2O} = \frac{M_{w,H_2O}}{2F} R_{an} \tag{11}$$

2.4 Energy Transport Process

The governing equation of energy is defined as in Equation 12, [11].

$$(\rho C_p)_{eff} \frac{\partial(T)}{\partial t} + (\rho C_p)_{eff}(v \cdot \nabla T) = \nabla \cdot (k_{eff} \nabla T) + S_T \tag{12}$$

In the GDL the possible heat source terms are shown by Equations 13 and 14 [12]

$$S_T = I(\rho C_p)_{eff} = (1 - \varepsilon)\rho_s C_{p,s} + \varepsilon \rho C_p \tag{13}$$

$$(\rho C_p)_{eff} = (1 - \varepsilon)\rho_s C_{p,s} + \varepsilon \rho C_p \tag{14}$$

Thermal conductivity for porous media (GDLs) is defined by equation 15, [12].

$$k_{eff} = -2k_s + \left[\frac{\varepsilon}{2k_s + k_g} + \frac{1 - \varepsilon}{3k_s}\right]^{-1} \tag{15}$$

The source term in the gas channels is given by Equation 16.

$$S_T = -\sigma A_{fg}(x_{sat} - x_{H_2O(g)})\Delta h_{fg} \tag{16}$$

Evaporation coefficient σ is given by Equation 17 [13], [14].

$$\frac{\sigma c_p}{\alpha} = \left[\frac{D \rho c_p}{k(1 + x)}\right]^{1-n} \left(\frac{V_h}{V_d}\right)^{m-n} \frac{\frac{M_w}{M_g} + x}{x_{sat} - x} ln \frac{\frac{M_w}{M_g} + x_{sat}}{\frac{M_w}{M_g} + x} \tag{17}$$

In the GDLs, heat sources are accounted for by Equation 18,

$$S_T = \frac{{i_e}^2}{{k_s}^{eff}} - \sigma A_{fg}(x_{sat} - x_{H_2O(g)})(\Delta h_{fg}) \tag{18}$$

In the CLs, the source term is given by Equation 19 [13],

$$\begin{aligned} &S_T \\ &= |j|\left[|\Delta V_{act}| - \frac{T\Delta S}{nF}\right] + \left(\frac{{i_m}^2}{{k_m}^{eff}} + \frac{{i_e}^2}{{k_s}^{eff}}\right) \\ &- \sigma A_{fg}(x_{sat} - x_{H_2O})(\Delta h_{fg}) \end{aligned} \tag{19}$$

S_T includes the ohmic resistance only and is given by Equation 20,

$$S_T = \frac{i_m^2}{k_m} \tag{20}$$

2.5 Water Transport Process

It seems that in PEMFC transport processes, water fraction content is one of the most critical elements in finding the distribution of current density in the membrane electrode assembly since it gives exact electrolyte potential distribution [15], [12]. The

conservation of liquid water in the processes is in terms of liquid saturation and is given by Equation 21 [12].

$$\nabla \cdot \frac{\eta_{g,} K_{rl}}{\eta_l K_{rg}} u_g = \nabla \cdot (\rho_l D_c \nabla s) - S_l \quad (21)$$

D_c is expressed by Equation 22,

$$D_c = \frac{K K_{rl}}{\eta_l} \frac{dp_c}{dS} \quad (22)$$

2.6 Electrical Charge Transport Process

The charge conservation principles in PEMFC are applied in the membrane, the CLs and the GDLs. The governing equations for the conservation of electrical charge can be written as in Equations 23 and 24, respectively [16]:

$$\nabla . (\sigma_s \nabla \emptyset_s) = S_{\emptyset_s} \quad (23)$$

$$\nabla . (\sigma_m \nabla \emptyset_m) = S_{\emptyset_m} \quad (24)$$

$\emptyset_m$ in $S_{\emptyset_m}$ is found from empirical relation given in Equation 25 [16],

$$\emptyset_m = (0.513\lambda - 0.326)\, exp\left[1268\left(\frac{1}{303} - \frac{1}{T}\right)\right] \quad (25)$$

3. METHODOLOGY

The objective of this study was to find the effect of cooling channels and heat spreaders on the fuel cell performance by applying the CFD process. The expected results were to show changes in terms of current density, temperature distribution and water content and distribution for the models. The methodology adopted was such that transport process equations described in the previous section were solved for a single cell. The CFD processes simulates the gas flows through channels, inflows and outflows generated by electrochemical reactions, diffusion through permeable media, proton flows via proton conducting PEM, electron flow through electrically conducting cell components, H_2O flow through PEM, H_2O flow through permeable CLs and GDLs, heat transfer and degradation of components. The study was carried out by running the model with varying cathode/anode potentials, hydrogen and air flowrates and pressures. In addition, some experiments were run on a fuel cell system to provide baseline data to the CFD model and to develop polarization curves for comparison purposes.

A CFD model of the Fuel Cell was developed using Ansys Fluent. The paper compares results between a model using a) hydrogen and air flows in the channels, b) hydrogen and air channels with cooling, and c) hydrogen and air channels with cooling and heat spreaders. The models were run independently, and the performances were compared. The parameters that were varied included voltages, hydrogen flow rates and pressure as shown in Table 1.

4. THE CFD MODEL OF PEMFC

4.1 Assumptions

These assumptions were made in the numerical simulations

i. Fuel cell works in steady-state conditions.
ii. The incompressible gas mixture and ideal fluid.
iii. The laminar flow in the channels.
iv. Non-Isothermal conditions.
v. Catalyst layers are reactive boundaries.
vi. Isotropous and homogeneous membrane and electrodes.
vii. The membrane cannot be penetrated by gas.
viii. Ohmic losses in the gradient diffusion layers and current collectors are ignored

4.2 Modelling

The CFD model has multiple straight channels cut on the current collector plates. The cell has seven components namely the two current collectors, two GDLs, two CLs and a membrane as shown in Table 2.

The CFD process carried out in this study is depicted in figure 3. The process began with pre-processing which consists of geometry creation and mesh generation. This was followed by physics setup and then description of boundary conditions before solution and convergence was obtained. The post processing describes analysis of the results and visualization.

4.3 The Geometry

The flow channels were designed to be straight and parallel. The model in figure 4a is a system with no separate cooling. Figure 4b depicts the models with a separate cooling channel adjacent to the air flow channels. Figure 4c shows the model with both the cooling channels and the heat spreader. The heat spreader is located between the air channel and the coolant channels. The heat spreader in this model uses liquid coolant (glycol with water mixture) with lower flow rate than in the coolant channels as shown in Table 1. The air channels were designed to be triangular in cross sectional shape. Some research has shown that other shapes like the rectangular cross section perform a little better in terms of performance, in this study particular focus was on the incorporation of cooling channels and heat spreaders without increasing the thickness of the cathode current collector hence the use of triangular channels.

Table 1. **Variable** p**arameters**.

Cell type	With no cooling variables	With cooling only	With cooling and spreader
Flow rates	H_2 :1 x 10^{-6} kg/s – 6 x 10^{-6} kg/s Air :1 x 10^{-5} kg/s – 6 x 10^{-5} kg/s		
		Coolant 5m/s	Coolant 5m/s Spreader fluid 2m/s
Pressure	60000 – 100 000 pascals		
Voltage	0.57 v – 0.89 v		
Temperature	Cell working temp 333 K Coolant and spreader liquid at room temperature of 300 K		
Results	Current density, Temperature, H_2O mass fraction		

Table 2. PEMFC Components and specifications.

Parts	No	Material	Density (kg/m^3)	Specific Heat J/kg-k	Thermal Conductivity W/m-k
Current collectors	2	Aluminium	2710	921	205
GDL	2	Carbon	2000	840	10.1
Catalyst	2	Platinum	387	770	71.6
Membrane	1	Nafion	1970	1100	0.27

Table 3. Components sizes

Components	Dimensions (length x width x thickness) mm
Current collectors	200 x 40 x 0.5
Flow channels	200 x 1 x 0.25
Membrane	200 x 40 x 0.05
Catalyst	200 x 40 x 0.01
Gradient diffusion layers	200 x 40 x 0.15

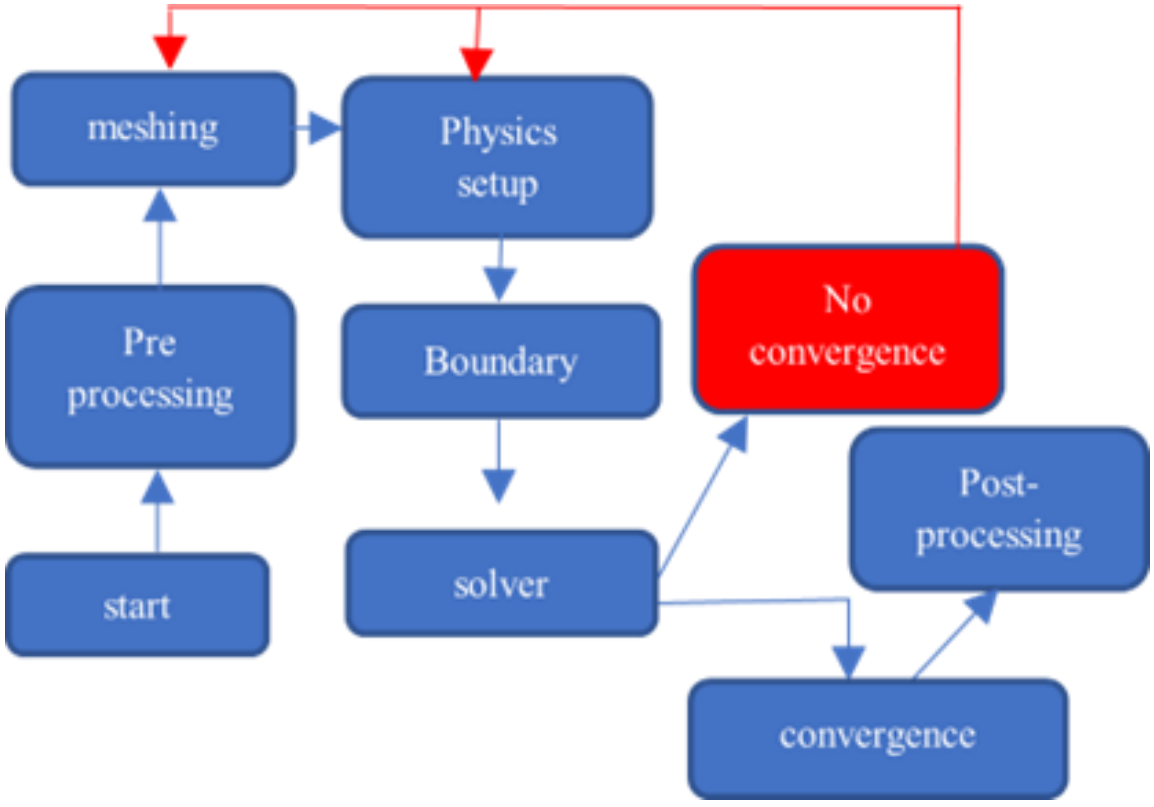

Fig. 3. CFD process flow diagram.

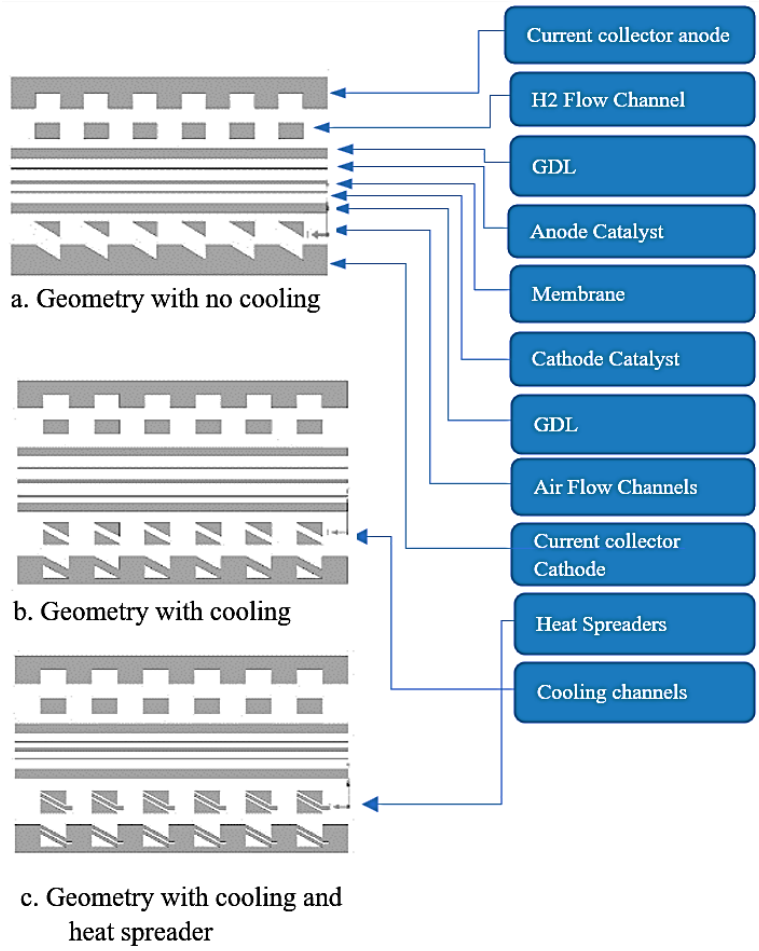

Fig. 4. Cross section representation of geometry configurations.

4.4 Meshing

This was the process of subdividing the homogeneous geometric space into discrete topological cells. In this study a structured hexahedral mesh was used. Though hexahedral meshing takes a long time to generate unlike other meshes such as tetrahedral mesh, the advantage is that they produce faster computational results. The three geometries described in Figure 5 generate meshes in the range of about 485 355 elements and 674 4355 nodes.

4.5 Mesh dependency study

The mesh independent study was done by running the simulation at 0.89 V at increasing the mesh density until the current density was constant as shown in Figure 5.

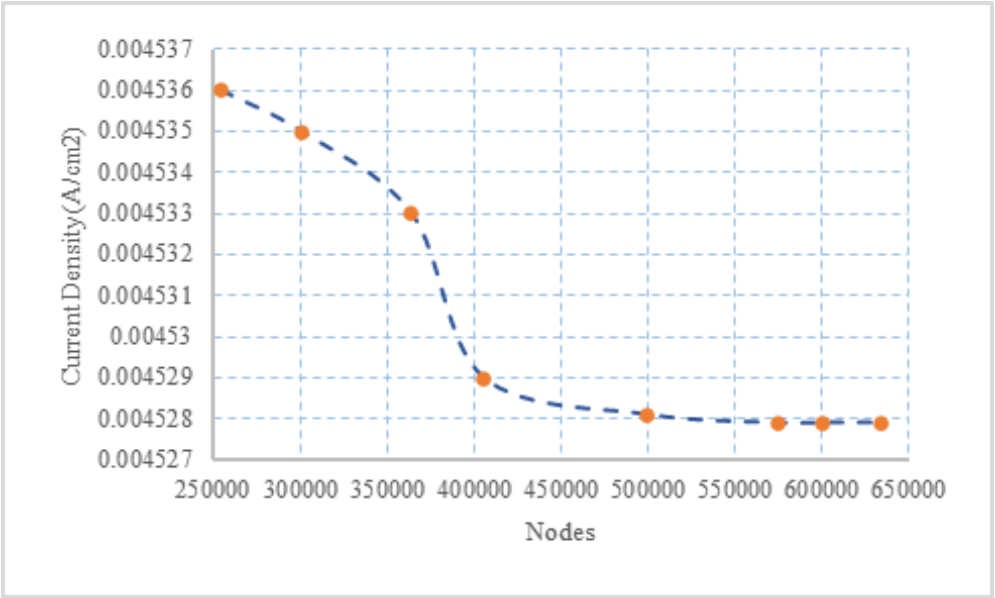

Fig. 5. Mesh independent study.

4.6 Solver

The simulation process utilized the pressure-based solver as opposed to the density-based type. The density-based option is a slow process because it solves the equations simultaneously and therefore uses a large amount of computing memory. However, the pressure-based solver was chosen because it is generally suitable for incompressible and mildly compressible flows.

4.7 Convergence

Convergence of the simulation depends on different factors, the major one being available computing resources. The computer used in this simulation is a 9th generation Intel Core i7 with a 3.4 GHz processor and a 16 GB of RAM. It took an average of 3500 iterations and 8 hours for convergence to be reached. The convergence was judged by observing the residuals. The absolute criteria of all the residual were set to 1e-06. Moreover, the quantity of interest in this simulation is current density both in the anode and cathode. Convergence was decided when the values of current density stayed the same indefinitely.

5.0 RESULTS AND ANALYSIS

5.1 Polarization Curves

Figure 5 shows the polarization curves derived from the experiment and those from the CFD model. There was a minor difference between the CFD model and experimental. This was shown as the experimental curve diverges at the current density values greater than 0.14 A/cm^2 which is at concentration losses. This is like the results obtained by Youssef *et al* [2] and explained as a familiar characteristic of a single-phase model whereby the result of lowered air flow due to the increase of water at the cathode side at higher current densities cannot be described. It was also observed that the experimental experiences rapid rate of activation losses as compared to the CFD model in the range of 0 to 0.05 A/cm^2.

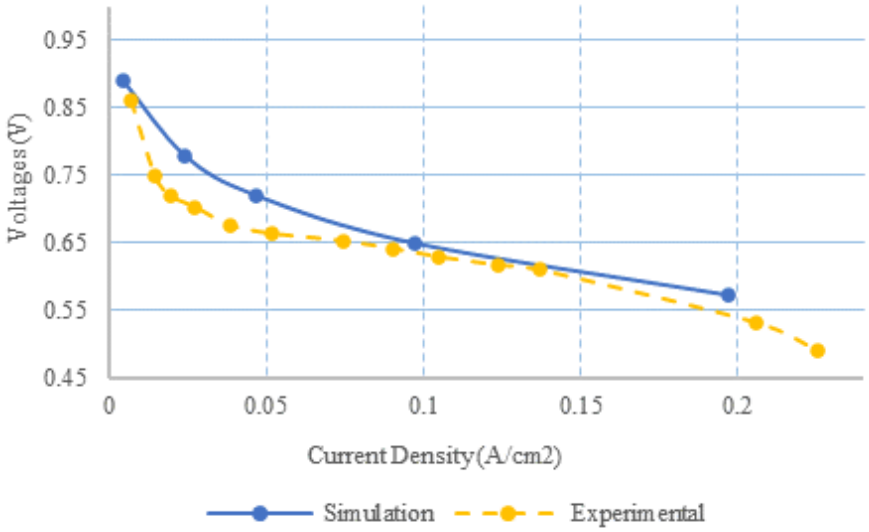

Fig. 5. Polarization curves for experimental and simulation.

Figure 6 shows the fuel cell temperature variations at the cathode catalyst and GDL zones for different flowrates. This shows that the non-cooled cell had a higher temperature of 333 K and remained just about constant as the flowrate was increasing. The presence of a separate cooling channel provided an average temperature of the cell at 323 K signifying a drop of 10 degrees whereas the cell with a heat spreader and cooling reduces the temperature to 321 K. The temperature of all the models remained almost constant as hydrogen flow rate increased therefore the results shows that hydrogen flow rate has little to no effect on the operating cell temperature. The heat spreader acts as a secondary cooling channel while also helping to spread the temperature of the cell and this help create a homogenous environment for electrochemical reaction in the reaction region.

A major part of this research was to improve the distribution of temperature in the fuel cell, but CFD simulation was also used to observe the formation of water content as the hydrogen flow rate increases with the introduction of cooling and heat spreader. Figure 7 depicts how increasing H_2 flow rates affect the H_2O mass fraction at the catalyst layer. There was more water mass fraction in a model with no cooling, and that reduced with cooling and with heat spreader. The existence of water in the fuel cell components is very critical. Too much water is not desirable and if not appropriately removed, there will be a restriction of the O_2 supply, and this will cause the fuel cell to overheat and subsequently dry out the cell [17]. Although the highest mass fraction reads about 0.11, which is also low and may not restrict the oxygen flow, the presence of cooling and heat spreader channels seems to demonstrate reduction of the accumulation of water in the catalyst and GDL layers.

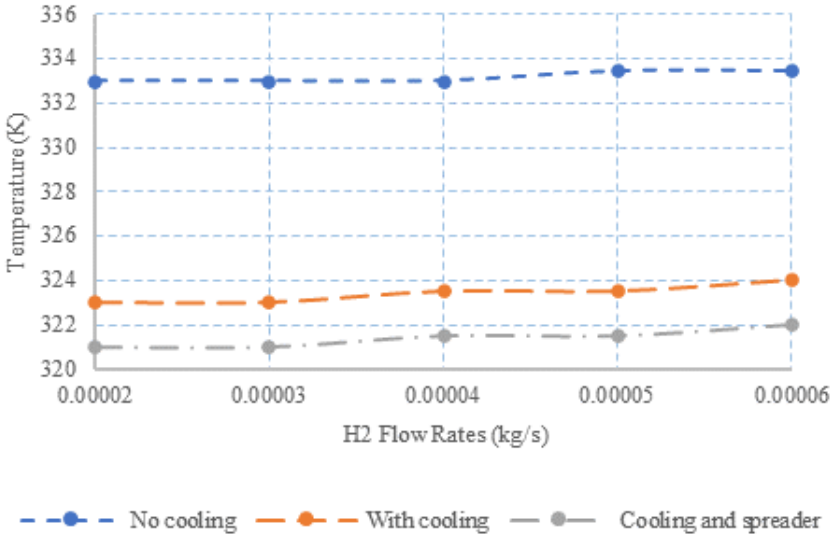

Fig. 6. The effect of H_2 flow rates on temperature (*Initial temperature at 333K, voltage at 0.89v)*.

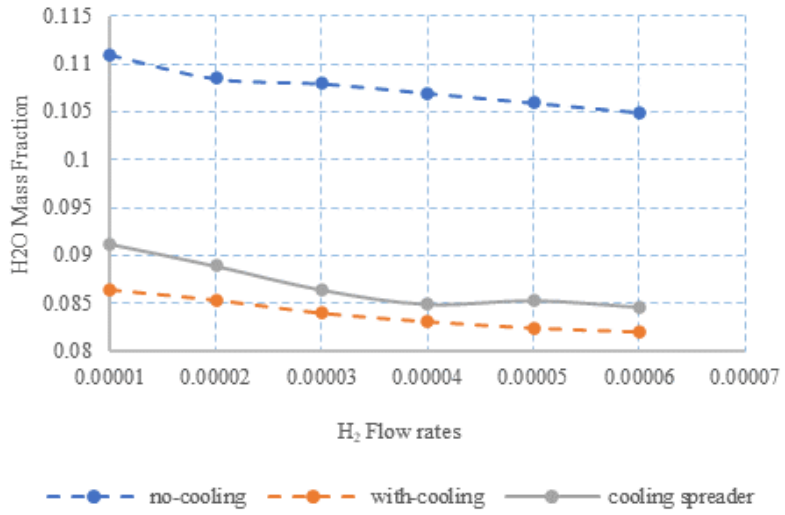

Fig. 7. Variation of H_2O mass fraction with H_2 flow rates.

Figure 8 shows the significance of pressure variations to the formation of water mass fraction in different cell configurations. Water mass fraction seemed to be decreasing as the pressure was increased. This observation compares to similar research carried out by Chen, *et al* [18], who found that water mass fraction decreases with pressure increase in the channels. It means that the fuel cell operating at a higher pressure reduces the water content problems. There is lower water content for the model with cooling while the one with heat spreader shows a little higher water content than the system with cooling but much lower than the one without cooling. The significance of the results meant that the cooling and heat spreader helped reduce the water content around the gradient diffusion layer region. This behavior could be associated with the temperature homogeneity created by the presence of cooling channel and heat spreader. The temperature homogeneity reduces some pockets of water content created by temperature variations in the non-cooled model.

The relationship between cell voltage and water mass fraction is shown in Figure 9. The relation shows that as cell voltage increases the mass fraction decreases (in the range of 0.13 to 0.1 at a margin of 0.57 V to 0.89 V) and this is comparable to the study conducted by Ahmadi N. e*t al* [19]. This is also confirmed by Yuan *et al.* [20] that the amount of water increases with the reduction in the voltage. The presence of the cooling channels and the heat spreaders made a difference in the saturation of the GDL region. The model with no cooling has a higher water content as compared to the ones with cooling and spreader and the one with cooling only respectively.

Figure 10 depicts the changes in water mass fraction as current density changes. The three graphs show that at low current densities the water content is lower at the cathode GDLs mainly because of back diffusion transfer towards the anode. At higher current densities the observation is that water content rises slightly due to electro osmotic drag.

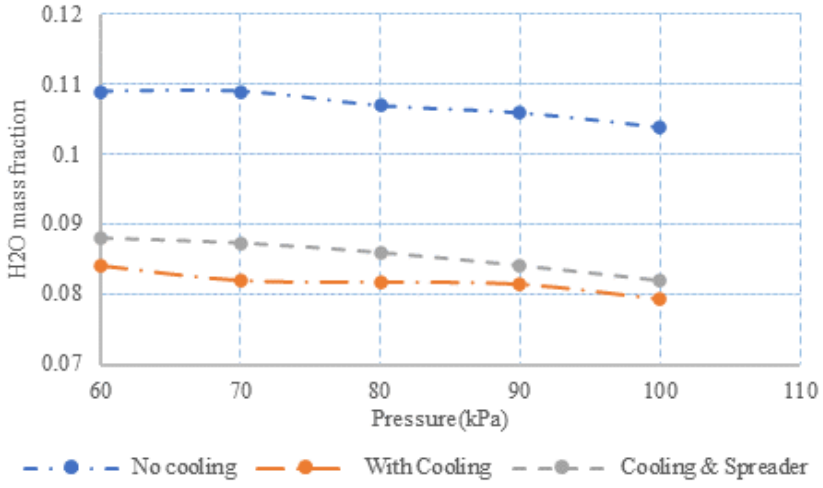

Fig. 8. The effect of pressure on H_2O mass fraction.

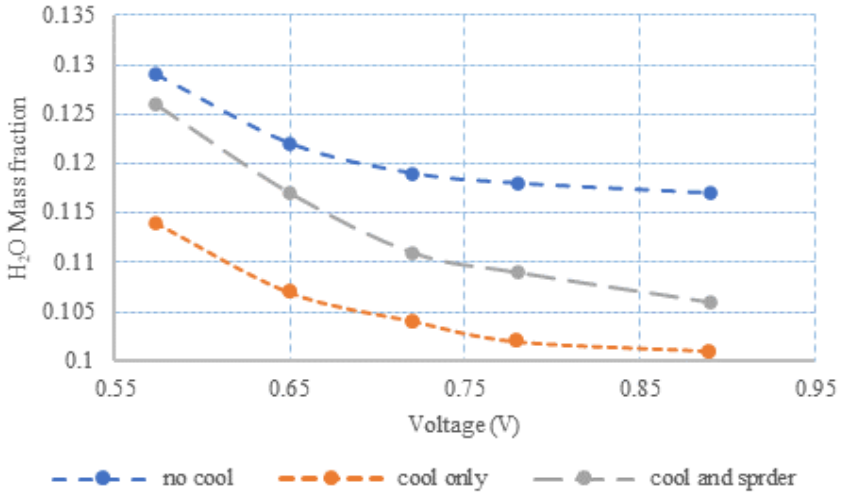

Fig. 9. The effect of voltage on H_2O mass fraction.

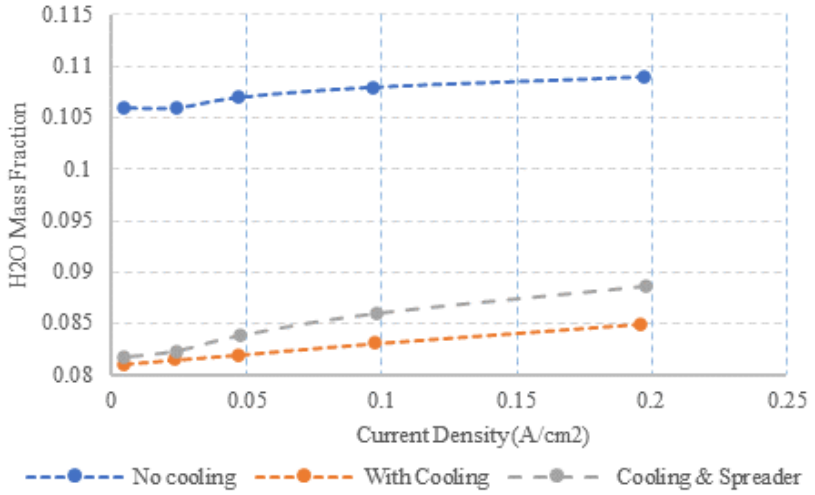

Fig. 10. The effect of current density on H_2O mass fraction.

Current density is directly proportional to pressure as shown in Figure 11. The rate of increase was similar for all the models as the pressure was increased. The relationship observed from the graphs could be represented as $y = 0.01x + 0.076$, where y and x represent the current density and the pressure respectively. It seemed the heat spreader in the model slightly helped in the increased current density as compared to the other models. From Figures 6-10, it is evident that incorporating cooling and heat spreader seemed to slightly enhance the performance of PEMFC. Increasing operating pressure usually improves cell performance in terms of power density and voltage [21]

The increase of hydrogen fuel flow rate causes gradual increase in fuel cell power as shown by an experimental graph Figure 12. The experimental graph begins lower and rises until it flattens signifying that as the fuel cell is started, it builds up power until it reaches a constant value. For the simulations power was constant as hydrogen flow was increased. This proves that a continuous increase in hydrogen flow does not translate to an indefinite increase in power because the cell can use a limited hydrogen amount and the remaining is recycled.

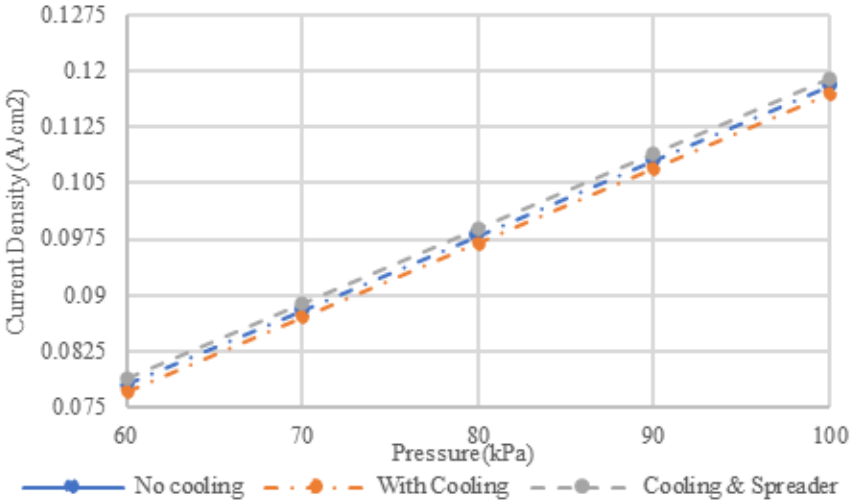

Fig. 11. The effect of pressure on current density.

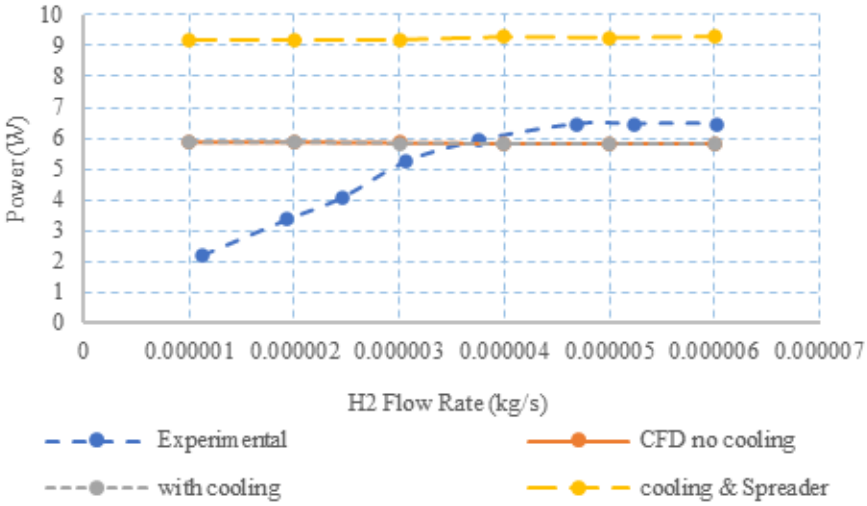

Fig. 12. The effect of pressure on current density.

Figure 13 compares temperature distributions between the different models at the same plane of the cross section of the model. The results show that the model without cooling did not experience temperature reduction as the other two models did. There was an influence of the presence of cooling channel and heat spreader in the distribution of temperature on the cross-section of the cell. In the model with cooling and heat spreader there was a significant heat distribution improvement along the channel's cross sections as also in the model with cooling channel. The introduction of spreader channels proves to be important in spreading heat away from reaction zones.

Hydration of PEMFC is important for achieving optimum performance and durability [22], [23]. Transport and formation of water content in a fuel cell can happen in electro osmotic drag (EOD), back diffusion from the cathode to the anode side and though electrochemical reactions. Figure 14 presents mass factions of water in the cell at 0.72 V. The model with heat spreader shows less amount of water content towards the anode compared to the cathode components. There was also significant water content in the air flow channels showing that the cooling effect of the spreaders caused water condensation into the channels. At higher temperature in the non-cooled model the water content is caused by electrochemical reactions and back diffusion causes water to be transferred across into anode side. The model does demonstrate that the extra cooling channels can be effective in reducing water content in the fuel cell and this could be beneficial for fuel cells operating at higher temperatures and current densities.

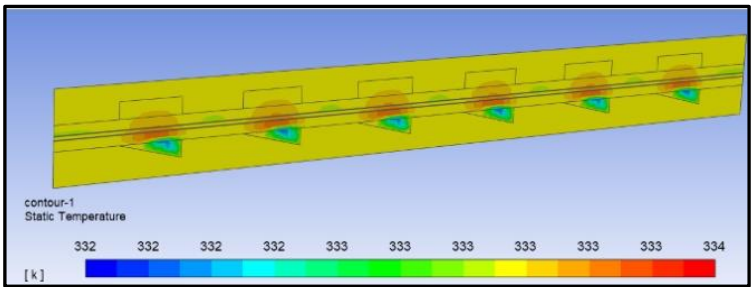

(a) Model with no cooling

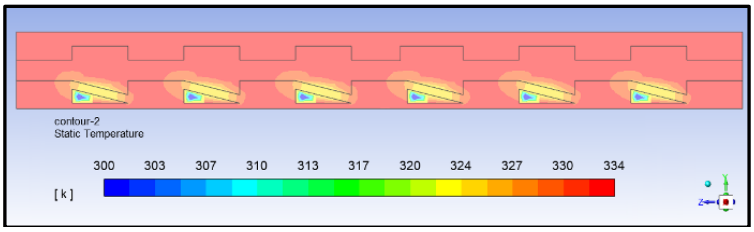

(b) Model with cooling

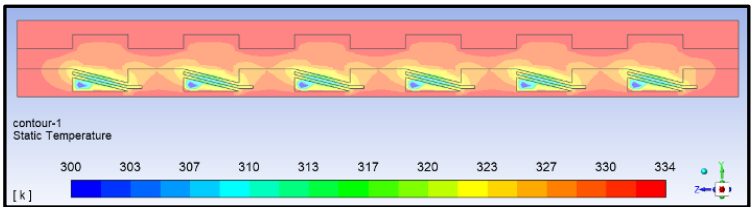

(c) Model with cooling and spreader

Fig. 13. Temperature distributions in PEMFC.

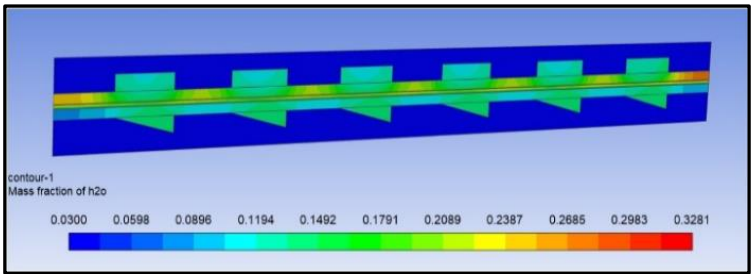

(a) No Cooling

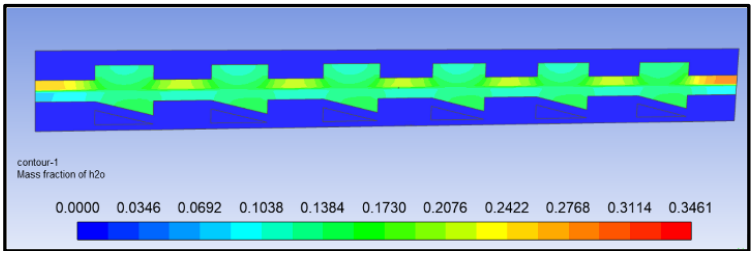

(b) With Cooling

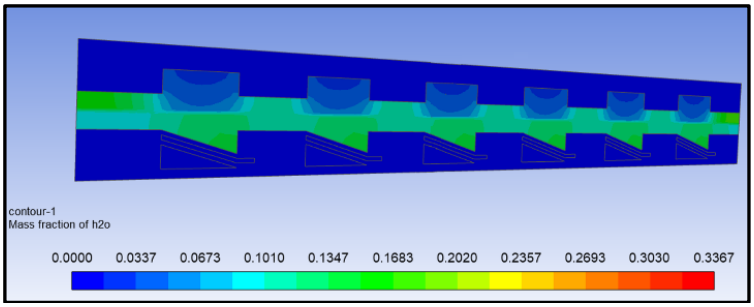

(c) With Cooling and Spreader

Fig. 14. H_2O mass fractions in PEM fuel cells.

Figure 15 shows the relationship between coolant velocity to current density. Other similar studies [24] shows that an increase in flow rate of coolant in cooling channels causes an increase in current density. This is evident in Figure 14 showing a slight increase in current density as coolant velocity increases. This could be due to improved heat distribution in the reaction zones hence improving the rate of electrochemical reactions

Figure 16 shows the effect of spreader liquid velocity on current density. Compared to the coolant channels the relationship in the spreader depicts a near straight line. As the liquid velocity is increased the current density slightly increases linearly. This could signify similar causes of improved thermal distribution in the GDL, membrane and catalyst zones hence improved electrochemical reactions.

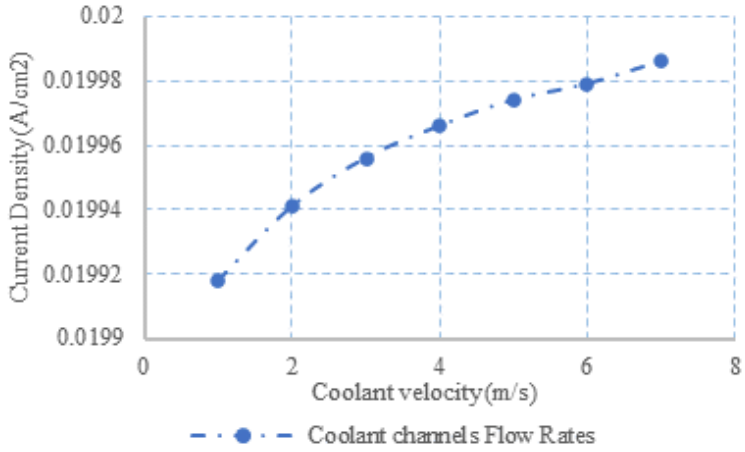

Fig. 15. Effect of coolant velocity on current density.

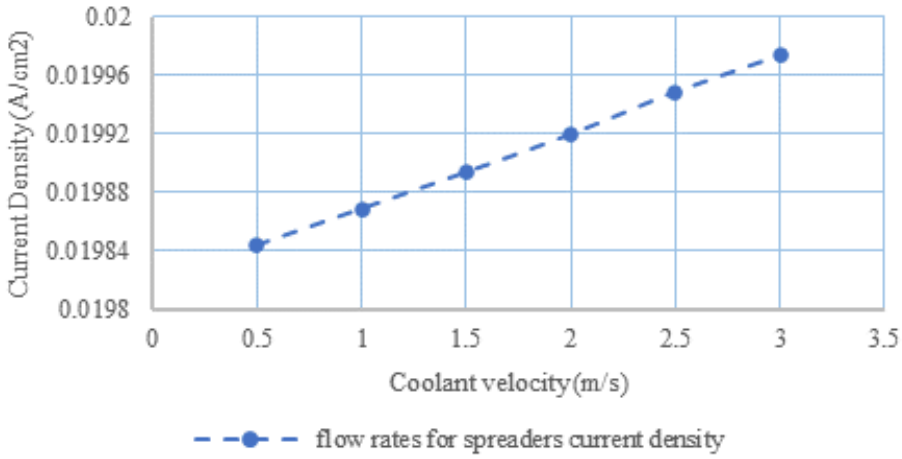

Fig. 16. Effect of coolant velocity on current density.

6. CONCLUSIONS

The paper presented the significance of the presence of separate cooling channels and heat spreaders in the fuel cell. The model was implemented in Ansys Fluent to get the results and analysis. The simulations were run using different input variables, namely pressure, voltage, and fuel flow rate. The purpose was to find how the incorporation of cooling channels and heat spreaders affect the performance of the fuel cell mainly in terms of current density, temperature distribution and water saturation in the MEA region. The heat spreader in this study presented a new alternative way of cooling by using a heat transfer liquid running at lower velocities to help spread heat from MEA region.

- Cooling channels influence the temperature of the cell, and the presence of heat spreader helps to distribute heat across the fuel cell as shown in the cell cross section in Figure 11.
- The presence of heat spreaders and cooling channels demonstrates the reduction of water content as demonstrated in figures 8, 9 and 10. For low current densities this may be insignificant but for higher current densities the introduction of this channels may be useful in reducing saturation pressure in the cathode GDL and catalyst zones.
- It also observed that apart from the primary intended function of heat distribution the heat spreaders also act as secondary cooling channels as evidenced by reduced temperatures in the MEA region.

Future work may expand the model to a multi-phase being able give detailed liquid and gas flow

characteristics in the cell. The study also could simulate a stack instead of a cell so that temperature distribution inside a stack will be well analysed because the single cell simulation doesn't present precise temperature variation in a stack of cells.

NOMENCLATURE

ρ	effective fluid density
v	inherent fluid velocity vector
ε	porosity
S_m	mass transport source term
$\boldsymbol{p}$	fluid pressure vectors
μ^{eff}	average viscosity of mixture
S_{mm}	momentum source term
K_p	hydraulic permeability of GDL, CL or membrane
μ	effective viscosity
x_m	volumetric fraction for CL
K_f	electrokinetic permeability
c_f	fixed charge concentration
n_f	sulfonic acid ions charge number
F	Faradays constant
$ø_m$	phase potential ionomer
D_j	effective mass diffusivity of species j
y_i	mass fraction of the i^{th} species of hydrogen, nitrogen, oxygen and water vapor
T_0	temperature of the binary diffusion coefficient
T	temperature of the fuel
ε_{eff}	effective porosity
s	liquid saturation fraction
M	molecular mass
F	Faraday constant
R_{an}	current density exchange, anode
R_{cat}	current density exchange, cathode
C_p	mixture average specific heat capacity
T	cell temperature, k_{eff} is the thermal conductivity
S_T	volumetric source
eff	effective property for the porous media
ρ_s	density
$C_{p,s}$	specific heat capacity of the solid state
k_{eff}	effective thermal conductivity (GDLs)
k_s	solid matrix thermal conductivity
k_g	gaseous phase conductivity
σ	evaporation coefficient
A_{fg}	surface area per unit volume of phase-change
x_{sat}	maximum mass fraction, dry gas water vapor
$x_{H2O(g)}$	water vapor fraction in dry gas
Δh_{fg}	the heat of evaporation
σ	determined from the Lewis factor $\sigma c_p/\alpha$
α	heat transfer coefficient between gas and water surface
D	water vapor diffusion through gas
c_p	heat capacity
k	humid gas thermal conductivity
x	water vapor fraction in dry gas
V_h	humid gas kinematic viscosity
V_d	dry gas kinematic viscosity
M_w	H_2O molecular mass
M_g	Gas molecular mass
m,n	coefficients which are about 0.75 and 0.33 respectively
i_e	current density
k_s^{eff}	effective electric conductivity (GDL)
j	transfer current density
ΔV_{act}	activation overpotential
i_m	is the ionic current density
$k^{eff}{}_m$	effective ionic conductivity of (CL, ionomer phase)
K_{rl}	liquid water relative permeability
K_{rg}	gaseous water relative permeability
η_l	liquid water viscosity
η_g	gaseous water viscosity
u_g	velocity vector for the gaseous mixture
D_c	diffusivity of liquid saturation
K	absolute permeability
$\frac{dp_c}{dS}$	gradient of capillary pressure with respect to saturation
$ø_s$	potential for solid phase
$ø_m$	potential for the electrolyte phase
λ	membrane water content

REFERENCES

[1] Ionescu V., 2016. Simulating the effect of gas channel geometry on PEM fuel cell performance by finite element method. *Procedia Technology, Romanian Journal of Physics*, 713–719.

[2] Carcadea E., Varlam M., and Ingham D.B., 2018. The effects of cathode flow channel size and operating conditions on PEM fuel performance: A CFD modelling study and experimental demonstration, *International Journal of Energy Research* 42(8): 2789-2804.

[3] Wu H., Kang D., and Perng S., 2017. Effect of rectangular ribs in the flow channels of HTPEM fuel cell by a three-dimensional model. *Energy Procedia*, 1376-1381.

[4] Liu H., Li P., Hartz A., and Wang K., 2015. Effects of geometry/dimensions of gas flow channels and

operating conditions of high temperature PEM fuel cells. *International Journal of Energy Environmental Engineering*, 75 – 89.

[5] Lee C.S. and S.C. Yi. 2004. Numerical methodology for proton exchange membrane fuel cell simulation using computational fluid dynamics technique. *Korean J. Chem. Eng.* 21(6): 1153-1160.

[6] Gao F., Blunier B., and Miraoui A., 2012. *Proton exchange membrane fuel cells modeling*, pp47-48. London: ISTE Ltd and John Wiley & Sons Inc.

[7] Ionescu V., 2014. Finite element method modeling of a high temperature PEM fuel cell. *Romanian Journal of Physics*, 285–294.

[8] Catlin G., 2010. *PEM fuel cell modeling and optimization using a generic algorithm* [PhD thesis], Department of Mechanical Engineering, University of Delaware, USA

[9] Le T., 2003. *Fuel cells: The epidemic of the future*, Indiana Institute of Technology, Institute of Electrical and Electronics Engineers, pp: 505-510.

[10] Wang Y., 2008. Modeling of two- phase transport in the diffusion media of polymer electrolyte fuel cells. *Journal of Power Sources* 185: 261–271.

[11] Cao T., Lin H., Chen Li., He Y., and Tao W., 2013, Numerical investigation of the coupled water and thermal management in PEM fuel cell. *Applied Energy* 112: 1115–1125.

[12] Bosnjakovic F., 1965. *Technical Thermodynamics*. Holt Rinehart and Winston, New York, USA.

[13] Ji M. and W. Zidong. 2009. A review of water management in polymer electrolyte membrane fuel cells. *Energies* 2: 1057- 1106.

[14] Hu M., Gu A., Wang M., Zhu X., and Yu L., 2004. Three-dimensional, two-phase flow mathematical model for PEM fuel cell: Part I. model development. *Energy Conversion and Management* 45: 1861-1882.

[15] Webber A., Borup R., Darling R., Das P., Dursch T., and Gu W., 2014. A critical review of modelling transport phenomena in polymer electrolyte fuel cells. *J. Electrochem. Soc*. 161(12): F1254-F1299.

[16] Wang X., Duan Y., Yan W., and Peng X., 2008., Effects of flow channel geometry on cell performance for PEM fuel cells with parallel and interdigitated flow fields. *Electrochimica Acta*, 5335-5343,

[17] Chen S., Wu Y., Sun H., and Sun Z., 2011. Simulation of pressure effect on water in the cathode for the PEM fuel cell. In *2011 Second International Conference on Mechanic Automation and Control Engineering*, pp 2566-2569.

[18] Ahmadi N., Rezazadeh S., Yekani M., Fakouri A., and Mirzaee I., 2013. Numerical investigation of the effect of inlet gases humidity on the polymer exchange membrane fuel cell (PEMFC) performance. *Transactions of the Canadian Society for Mechanical Engineering* 37(1): 70-71.

[19] Lu J.B., Wei G.H., Zhu F.J., Yan X.H., and Zhang J.L., 2019. Pressure effects on PEM fuel cell performance. *Fuel Cells* 19(3): 225-241.

[20] Yuan W., Li J., Xia Z., Chen S., Zhang X., Wang Z., and Sun H., 2020. Study of water transport mechanism based on the single straight channel of proton exchange membrane fuel cell. *AIP Advances* 105206: 1-14.

[21] Lee P. and S. Hwang. 2009. Performance characteristics of a PEM fuel cell with parallel flow channels at different cathode relative humidity levels. *Sensors (Basel)*, pp. 9104 – 9121.

[22] Barbir F., 2012., *Fuel Cells: Theory and Practice*, 2nd edition, ISBN: 9780123983725. London: Academic Press.

[23] Yuan W., Li J., Xia Z., Chen S., Zhang X., Wang Z., and Sun H., 2020. Study of water transport mechanism based on the single straight channel of proton exchange membrane fuel cell. *AIP Advances* 105206: 1-14.

[24] Rahgoshay S., Ranjbar A., Ramiar A., and Alizadeh E., 2017. Thermal investigation of a PEM fuel cell with cooling flow field. *Energy* 134: 61-73.